Research Square

Preprints are preliminary reports that have not undergone peer review.
They should not be considered conclusive, used to inform clinical practice,
or referenced by the media as validated information.

Effects of Radial Electric Fields on Alpha Particle Confinement in the CAT-1 Levitated Dipole Device

Yunhui Liu

1501193797@qq.com

East China University of Technology

Zhao Wang

East China University of Technology

Teng Liu

East China University of Technology

Guoshu Zhang

East China University of Technology

Research Article

Keywords: Radial Electric Fields, Dipole Field, E×B

Posted Date: May 30th, 2026

DOI: https://doi.org/10.21203/rs.3.rs-9714947/v1

License: This work is licensed under a Creative Commons Attribution 4.0 International License.
Read Full License

Additional Declarations: No competing interests reported.

Effects of Radial Electric Fields on Alpha Particle Confinement in the CAT-1 Levitated Dipole Device

Yunhui Liu[1], Zhao Wang[1], Teng Liu[1], Guoshu Zhang[1]
[1]East China University of Technology, Nanchang, China
E-mail: 1501193797@qq.com

Abstract

Radial electric fields are known to arise from non-ambipolar transport in dipole-confined plasmas, yet their effects on high-energy alpha particle confinement remain systematically unexplored for compact levitated devices. This study employs test-particle simulations based on the parameters of the China Astro-Torus 1 (CAT-1) levitated dipole experiment to investigate how such fields influence alpha particle trajectories, losses, and slowing-down confinement. The key result is that a moderate radial electric field can increase the confined fraction of alphas by up to 40% within the ion slowing-down time, a substantial improvement for heating the background plasma. Furthermore, the confinement fraction varies systematically with the strength of the inner field (E_{in}) and the ratio of outer-to-inner field (κ), with high E_{in} and $\kappa > 1$ yielding optimal results. These findings suggest that tailoring the radial electric field profile offers a novel, knob-like handle for controlling alpha particle heating in dipole fusion concepts.

Keywords: Radial Electric Fields; Dipole Field; E×B

1 INTRODUCTION

A dipole magnetic field configuration has been proposed as a potential basis for a compact fusion reactor [1, 2]. In laboratory experiments such as the Levitated Dipole Experiment (LDX) and the Ring Trap 1 (RT-1), it has been demonstrated that a levitated superconducting dipole coil can stably confine a high-beta plasma with a self-organized peaked pressure profile [3, 4]. These successes have motivated further exploration of dipole-based fusion concepts, including the China Astro-Torus 1 (CAT-1) — a small-scale levitated dipole device designed to investigate D-D and catalyzed D-D fusion reactions [9].

In dipole-confined plasmas, radial electric fields are commonly observed. In early LDX experiments, such fields were attributed to non-ambipolar transport or unintentional electrostatic bias of the floating coil [5]. The direction of the radial electric field typically reverses near the plasma pressure peak: radially outward on the inner side of the peak and radially inward on the outer side [6–8]. The magnitude of the electric field can be estimated from toroidal plasma rotation speeds (100–200 km/s) measured in similar devices, corresponding to fields on the order of several kV/m in the mid-plane of CAT-1 (magnetic field 0.01–0.1 T). Despite the ubiquitous presence of such radial electric fields, their influence on the confinement of high-energy charged particles — and in particular on

fusion-born alpha particles — has not been systematically evaluated for compact levitated dipole devices.

This knowledge gap is important for two reasons. First, the stable confinement of high-energy alpha particles is crucial for effectively heating the background plasma and sustaining a fusion reaction in a dipole reactor. Second, if radial electric fields can significantly alter alpha particle orbits, they could provide a controllable "knob" to either enhance heating or mitigate losses. Indeed, in a dipole field, the $\mathbf{E} \times \mathbf{B}$ drift caused by a radial electric field can modify the particle drift trajectories, potentially reducing the radial excursion and thus avoiding collisions with the vacuum chamber or support structures.

In this paper, we address this gap by performing a systematic test-particle study of high-energy alpha particle confinement in the CAT-1 levitated dipole device, with and without a model radial electric field. The electric field profile is assumed to be purely radial and to reverse direction at a prescribed radius R_e, mimicking the experimentally observed reversal layer. The inner (E_{in}) and outer (E_{out}) field strengths are varied over a range of 0.5–5 kV/m, covering the estimated experimental regime. Using a full-orbit Boris integrator, we simulate the trajectories of thousands of alpha particles launched from different radii, with initial kinetic energies from 10 to 50 keV and pitch angles from $-90°$ to $90°$. Three loss channels (vacuum chamber, support rods, and the floating coil itself) are included based on the actual geometry of CAT-1.

Our key findings are as follows. (i) A moderate radial electric field ($\approx$5 kV/m) can increase the confined fraction of alpha particles by up to 40% within the ion slowing-down time, compared to the field-free case. (ii) The confinement improvement is most pronounced when the injection point lies outside the reversal layer (i.e., in the weak-field region). (iii) The confinement fraction increases with the magnitude of E_{in} and with the ratio $\kappa = E_{\mathrm{out}}/E_{\mathrm{in}}$; for $\kappa > 1$ the enhancement is particularly strong. (iv) The effect saturates when the reversal layer radius R_e exceeds about 2 m, but still yields a 6–12% improvement compared to the case without a reversal layer. These results demonstrate that the radial electric field is not merely a parasitic effect, but can be exploited as a practical means to control alpha particle heating in dipole fusion devices.

The remainder of this paper is organized as follows. Section 2 describes the CAT-1 device geometry, the magnetic and electric field models, the test-particle setup, and the Boris integration scheme. Section 3 presents the alpha particle trajectories, kinetic energy evolution, and magnetic moment behavior, comparing the cases with and without the radial electric field. Section 4 systematically examines the influence of the injection location, the inner-field strength E_{in}, the field-strength ratio κ, and the reversal layer radius R_e on the confinement fraction. Section 5 summarizes the main conclusions and discusses their implications for future dipole-based fusion experiments.

2 MODELING

2.1 The CAT-1 and its modeling

The China Astro-Toru 1 (CAT-1) is an experimental device that uses a dipole magnetic field to confine plasma, with its magnetic field generated by a magnetically levitated toroidal coil. The design parameters of the CAT-1 device require a plasma density greater than 5×10^{19} m^{-3}, a plasma temperature of up to 500 eV, a vacuum chamber diameter of 4 m, and a magnetic field strength on the coil surface of $\geq$5 T. In a dipole

magnetic confinement device, particles will collide with the vacuum chamber along non-closed magnetic field lines, causing losses due to collisions with the dipole field coils or support structures, and the energy of the particles is deposited onto the structure, causing damage to the structure body. Therefore, studying the influence of the radial electric field on the high-energy α particles confinement characteristics in the CAT-1 device is of great significance for the effective heating of plasma by high-energy particles within the slowing-down relaxation time, as well as for the protective design of the dipole field coils, the design of the vacuum chamber, and the design of the diverters.

Figure 1 plots the conceptual design of the CAT-1 device, the primary channels for particle collision losses, which encompass particle losses from collisions with the vacuum chamber, interactions with the support structure, and impacts against the dipole field coils. Here, it should also be noted that the attitude control coils, located above the top of the vacuum chamber, do not participate in particle collision losses. The specific design parameters of the CAT-1 device have been listed in previous articles [9, 11]. Table 1 provides the collision volume parameters for the three loss channels.

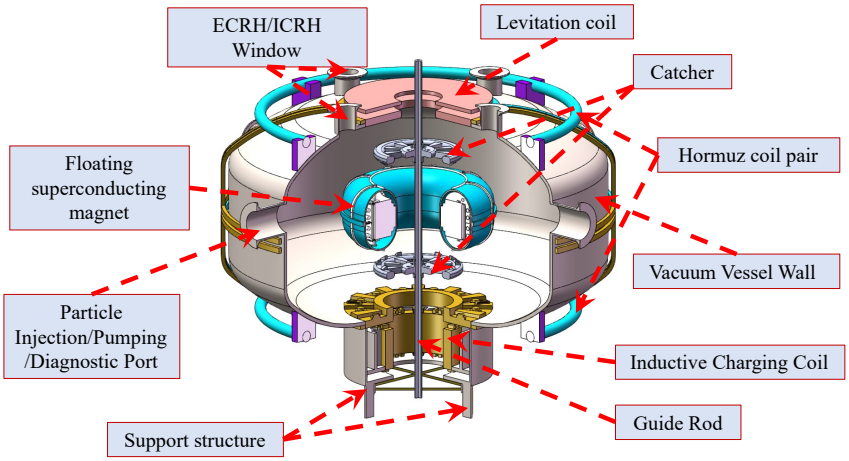


Figure 1: A schematic diagram of the CAT-1 structure.

Table 1: Collision volume parameters for the three loss channels.

Vacuum Chamber	Top Z_{Vt} (m)	Bottom Z_{Vb} (m)	Radius R_V (m)
	-1.5	2	3.8
Support Rod	Top Z_{St} (m)	Bottom Z_{St} (m)	Radius R_S (m)
	-2	2	0.1
Dipole Field Coil	Width W_{DC} (m)	Height H_{DC} (m)	Major radius R_{DC} (m)
	0.2	0.2	0.5

We have developed a full-orbit particle tracking code, named as (magnetic Dipole Field Particle tracking Code), that employs the Boris method for time advancement, and the current version does not include the effects of Coulomb collisions. We have conducted benchmark tests on modules such as magnetic field generation and particle motion. The choice of timestep $dt = 10^{-10}$ s resolves the alpha particle gyromotion with approximately 50 points per cyclotron period at 50 keV, ensuring accurate orbit integration while maintaining computational efficiency.

2.2 Generation of a radial electric field

In Abler's PhD thesis [12], it is theorized that the position of the electric field reversal coincides with the ECRH resonance layer, typically located in the laboratory dipole field devices. The multiple frequencies of ECRH are used to heat the plasma in the LDX or RT-1 devices; therefore the position of the conversion layer is consistent with the peak position of the plasma pressure.

The magnitude of the electric field can be estimated through the ideal Ohm's law. In the article by Guazzotto et al. [8], a toroidal plasma rotation speed of approximately 100 km/s to 200 km/s is given. In CAT-1, the magnetic field on the mid-plane is about 0.01 T to 0.1 T, thus the magnitude of the electric field is approximately 1 kV/m to 20 kV/m. To account for system redundancy, we select electric field values of 0.5 kV/m, 2 kV/m, and 5 kV/m as benchmarks to study the confinement time of alpha particles under different ratios of inner to outer electric fields across the reversal layer.

We assume that the electric field has no component in the Z direction, and the X and Y components of the electric field are independent of the Z coordinate. Then the expression for the distribution of the radial electric field is given by:

$$\begin{cases} E_x = \begin{cases} E_{\text{in}} \cos\theta, & R \le R_e \\ -E_{\text{out}} \cos\theta, & R > R_e \end{cases} \\ E_y = \begin{cases} E_{\text{in}} \sin\theta, & R \le R_e \\ -E_{\text{out}} \sin\theta, & R > R_e \end{cases} \\ E_z = 0 \end{cases} \tag{1}$$

where E_{in} represents the electric field strength inside the electric field direction conversion layer, E_{out} denotes the electric field strength outside the electric field direction conversion layer, θ is the angle between the observation point and the origin, and R_e indicates the radius of the electric field direction conversion layer. Figure 2 shows a schematic diagram of the electric field distribution on the X-Y plane.

2.3 Test particles and Boris algorithm

This study is based on the test particle method, where the motion of charged particles in an electromagnetic field satisfies the following equation:

$$\frac{d\mathbf{v}}{dt} = \frac{q}{m}\left(\mathbf{E} + \mathbf{v} \times \mathbf{B}\right) \tag{2}$$

$$\frac{d\mathbf{x}}{dt} = \mathbf{v} \tag{3}$$

where q represents the charge of the particle, m is the mass of the particle, $\mathbf{E}$ is the electric field vector at the particle location, and $\mathbf{B}$ is the magnetic field vector at the particle location.

The Boris-Buneman algorithm [13, 14] has one of the main advantages of not accumulating system energy error over time while maintaining accuracy. It is a standard algorithm for solving the motion of charged particles in electromagnetic fields, especially in plasma physics and particle simulation. The motion Eq. (2) for charged particles is

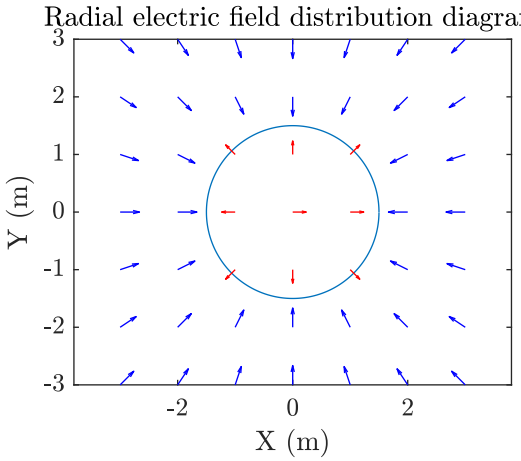


Figure 2: A schematic diagram of the radial electric field. The middle ring represents the position of the positive and negative conversion layer. The direction of the electric field in the layer is far away from the center of the circle like a red arrow, and the direction of the electric field outside the layer is towards the center of the circle like a blue arrow. The selected electric field strengths (0.5, 2, 5 kV/m) cover the range expected from toroidal rotation measurements in similar dipole devices [8], while the ratio $\kappa = E_{\text{out}}/E_{\text{in}}$ is scanned from 0.5 to 2 to systematically explore the effect of field reversal asymmetry. The conversion layer radius R_e is varied from 0 to 2 m to account for possible shifts of the ECRH resonance layer in experiments.

discretized, and its expression is as follows [15]:

$$\frac{\mathbf{x}_{k+1} - \mathbf{x}_k}{dt} = \mathbf{v}_{k+1/2} \tag{4}$$

$$\frac{\mathbf{v}_{k+1/2} - \mathbf{v}_{k-1/2}}{dt} = \frac{q}{m_0}\left(\mathbf{E}_k + \frac{\mathbf{v}_{k+1/2} + \mathbf{v}_{k-1/2}}{2} \times \mathbf{B}_k\right) \tag{5}$$

$$\mathbf{v}^- = \mathbf{v}_{k-1/2} + \frac{q}{m_0}\frac{dt}{2}\mathbf{E}_k \tag{6}$$

$$\mathbf{v}^* = \mathbf{v}^- + \frac{q}{m_0}\frac{dt}{2}\mathbf{v}^- \times \mathbf{B}_k \tag{7}$$

$$\mathbf{v}^+ = \mathbf{v}^- + \frac{2}{1 + \left(\mathbf{B}_k \frac{q}{m_0}\frac{dt}{2}\right)^2}\mathbf{v}^* \times \mathbf{B}_k \frac{q}{m_0}\frac{dt}{2} \tag{8}$$

$$\mathbf{v}_{k+1/2} = \mathbf{v}^+ + \frac{q}{m_0}\frac{dt}{2}\mathbf{E}_k \tag{9}$$

where $\mathbf{v}$, $\mathbf{x}$, $\mathbf{E}$, and $\mathbf{B}$ represent velocity, displacement, electric field, and magnetic field vectors, respectively. dt is the time step, and the subscript k represents the physical quantity of the kth time step.

3 THE INFLUENCE OF RADIAL ELECTRIC FIELDS ON ALPHA PARTICLE TRAJECTORIES

The CAT-1 is a physical experimental device and not directly applicable to D-^{3}He fusion nuclear reactions; the maximum vacuum magnetic field in the plasma region is less than

1 T, and thus the magnetic field cannot confine alpha particles with a kinetic energy of 3.6 MeV. The energy range for alpha particles in this paper is determined through the ideal Magnetohydrodynamic (MHD) scaling law. Once the density and magnetic field strength of a D-^{3}He fusion reactor are established, the energy of alpha particles, $T_{\rm cat}$, is calculated using the scaling law:

$$T_{\rm cat} = \frac{\left(B_{\rm cat}/B_{\rm fus}\right)^2}{n_{\rm cat}/n_{\rm fus}} T_{\rm fus}. \tag{10}$$

In the D-^{3}He fusion reactor, the magnetic field strength, plasma density, and temperature are 2 T, 2×10^{20} m^{-3}, and 75 keV, respectively. In the CAT-1 device, the magnetic field strength, plasma density, and temperature are 0.05 T, 1×10^{19} m^{-3}, and 500 eV, respectively. Therefore, the energy of alpha particles is approximately 45 keV. To account for system redundancy, we take the alpha particle energy of 25 keV as a reference and scan the alpha particle kinetic energy from 10 keV to 50 keV.

3.1 Trajectories without radial electric fields

To compare with the confinement of high-energy alpha particles under conditions that include a radial electric field, this paper first discusses the motion of high-energy alpha particles in the CAT-1 device during levitated operation without a radial electric field. During levitated operation in the CAT-1 device, the coupling of the magnetic field produced by the levitated coil and the dipole field coil results in an up-down asymmetric magnetic configuration, which changes in the period of the longitudinal adiabatic invariant. Concurrently, due to the lack of magnetic shear, particles move quickly along the magnetic field lines and collide with the vacuum chamber top (divertor), resulting in loss. Different from the magnetic mirror device, the levitated dipole field device has a closed magnetic surface structure, and when particles have a large parallel velocity, their trajectories will not have a magnetic mirror point, but will pass through the inner mid-plane of the coil to form a connected structure, thus confining the particles in the dipole field. Particles moving on the magnetic surface near the last closed flux surface (LCFS) are lost through the X-point along the magnetic field line, or particles with a larger Larmor radius collide with the side wall of the vacuum chamber and are lost.

To visually demonstrate the relationship between particle loss and injection position and angle, this section selects 5 points on the X-Z plane as the initial positions for particles and injects them at angles of 60° and 30° (the angle between the initial velocity and the magnetic field lines). It is assumed that the kinetic energy of the alpha particles is 25 keV, and the time step is chosen as $dt = 1 \times 10^{-10}$ s. The particle simulation time $T = 5 \times 10^{-4}$ s. Figure 3 shows the trajectories of alpha particles in the poloidal plane in the cylindrical coordinate system and the magnetic moments corresponding to the particles.

In Figures 3(a) and (b), the trajectory of high-energy alpha particles gradually changes from a quasi-periodic path to a disordered chaotic trajectory. Figure 3(d) plots the normalized magnetic moment $\bar{\mu} = \mu/\langle\mu\rangle$ of the five alpha particles over time (where the brackets $\langle\ldots\rangle$ denote a time average), showing that the normalized magnetic moment μ exhibits periodic variation and approximates to a constant within a particle cyclotron period when the particle throw position is on the side of strong magnetic field intensity. When the injection point moves radially outward along the mid-plane, the magnetic moment gradually becomes non-periodic. To compare the effect of the injection angle on

the trajectory of high-energy alpha particles, simulations were conducted under the same conditions for alpha particles with an injection angle of 60°, and the results are shown in Figure 4.

Under the condition of a 60° injection angle, the alpha particles injected close to the coil side experience an increase in their perpendicular velocity $v_\perp$ and a corresponding decrease in their parallel velocity $v_\parallel$. This results in an increased Larmor radius for the alpha particles, and a reduced latitude of precession along the magnetic field lines. The magnetic field strength within the particle's bounce region changes little, hence the change in its magnetic moment is more uniformly oscillatory compared to the case with a 30° injection angle. In contrast, particles injected away from the coil side still exhibit chaotic trajectories when the injection angle is altered.

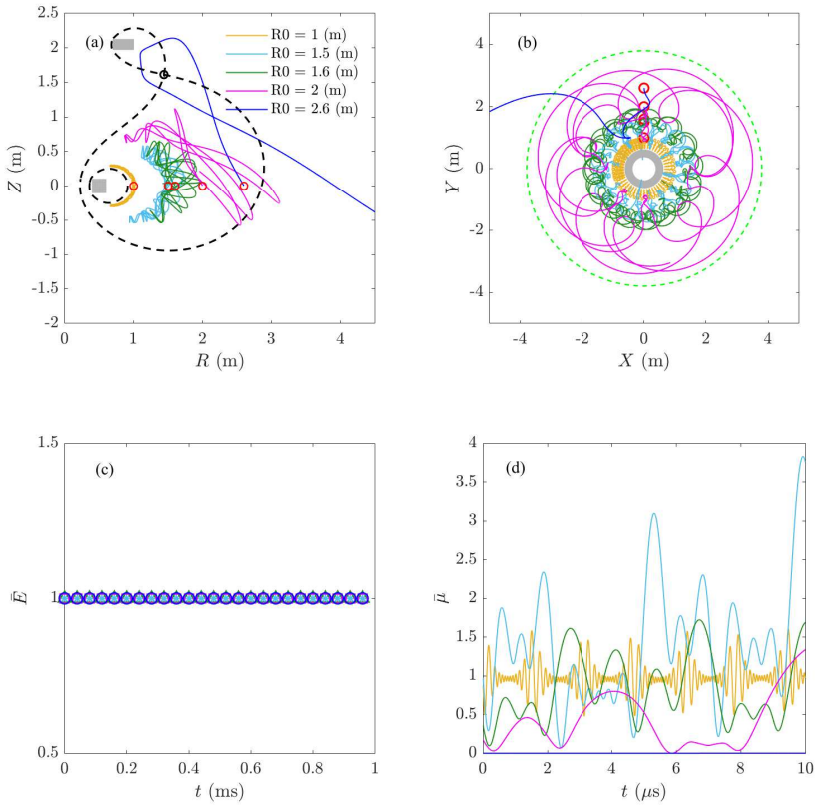


Figure 3: In the cylindrical coordinate system, the high-energy α particles at five different throwing points with a throwing angle of 30° without radial electric field are (a) RZ plane trajectory, (b) α particles in the Cartesian coordinate system. The orbit top view, α particles (c) kinetic energy and (d) normalized magnetic moment change with time. The transition from quasi-periodic to chaotic $\mu(t)$ for $R_0 \geq 1.5$ m signals the breakdown of adiabatic invariance.

The transition from quasi-periodic to chaotic magnetic moment behavior observed in Figures 3(d) and 4(d) reflects the breakdown of adiabatic invariance as the injection radius increases. For $R_0 \leq 1.0$ m, the particle remains predominantly in the strong field region near the coil, where the magnetic field inhomogeneity scale length is much larger than the Larmor radius. Consequently, the magnetic moment μ is conserved on

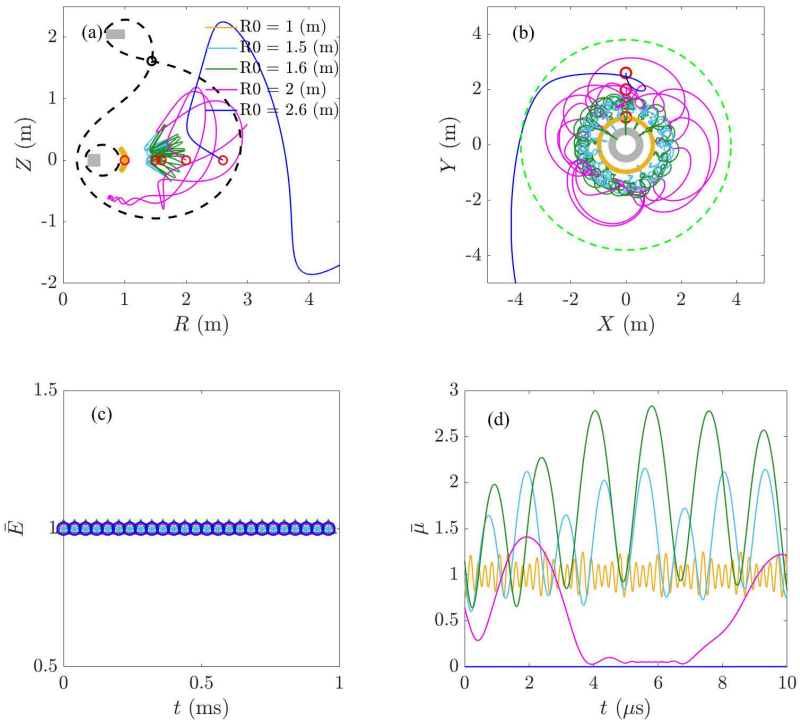


Figure 4: In the cylindrical coordinate system, the high-energy α particles at five different throwing points with a throwing angle of 60° without radial electric field are (a) RZ plane trajectory, (b) α particles in the Cartesian coordinate system. The orbit top view, α particles (c) kinetic energy and (d) normalized magnetic moment change with time.

the gyration time scale. For $R_0 \geq 1.5$ m, the particle traverses regions of weaker and more sheared field, particularly near the mid-plane periphery. In this regime, the gyro-averaging approximation breaks down, and μ exhibits non-adiabatic fluctuations. This loss of adiabaticity is the primary reason why particles injected at larger radii are more prone to chaotic orbits and eventual loss. It also sets the stage for the radial electric field to have a significant effect, as the $\mathbf{E} \times \mathbf{B}$ drift can partially reorder these chaotic trajectories.

3.2 The influence of radial electric fields on particle confinement

The primary focus of the study is on the influence of the radial electric field on particle trajectories, kinetic energy, and magnetic moments. Under the same initial conditions as the previous section, we introduced an electric field direction conversion layer with a radius $R_e = 1.5$ m, and the values of the electric field inside the conversion layer E_{in} and outside the conversion layer E_{out} are both equal to 5 kV/m. Figure 5 illustrates the trends in the basic properties of particles under the condition of a 30° injection angle.

With the addition of the radial electric field, the confinement of high-energy alpha particles in the weak field area outside the dipole field coil is improved. The radial electric field reduces the trajectory radius range of alpha particles, thus avoiding losses caused by collisions with the vacuum chamber wall due to large particle gyro-radius. In Figure 5(c), the kinetic energy of the particles exhibits a periodic-like pattern under the influence of the radial electric field. At the initial moment, when the direction of particle motion is opposite to the acceleration produced by $\mathbf{E} \times \mathbf{B}$ inside the conversion layer, the kinetic energy of the particles shows a periodic-like variation that first decreases and then increases over time. Conversely, when the direction of particle motion is the same as the acceleration produced by $\mathbf{E} \times \mathbf{B}$ inside the conversion layer, the kinetic energy of the particles shows a variation that first increases and then decreases over time. We also plot the trajectories of particles with a 60° injection angle in Figure 6. In the region of high magnetic field strength, particles exhibit the same variation pattern whether or not the radial electric field is included, but the total kinetic energy of the particles is altered due to the presence of the radial electric field. In the weak field area the radial electric field improves the confinement of the particles.

The improved confinement observed in Figures 5 and 6 can be understood through the effect of the $\mathbf{E} \times \mathbf{B}$ drift. In the presence of a radial electric field E_r, the drift velocity is $\mathbf{v}_E = (\mathbf{E} \times \mathbf{B})/B^2$, which for an axisymmetric dipole field has both poloidal and toroidal components. When the electric field reverses direction at R_e, the sign of $\mathbf{v}_E$ also reverses. Inside the reversal layer ($R < R_e$), $\mathbf{E}$ points outward, producing a drift that pushes particles toward larger R. Outside ($R > R_e$), $\mathbf{E}$ points inward, producing a drift that pushes particles back toward smaller R. This "push-pull" configuration effectively compresses the radial extent of alpha particle orbits, reducing the probability of hitting the vacuum chamber wall (located at $R = 3.8$ m). The effect is most pronounced for particles injected in the weak field region ($R_0 \sim 1.5$–2.5 m), where the magnetic field is too weak to confine them by itself. The periodic modulation of kinetic energy seen in Figures 5(c) and 6(c) arises from the work done by the electric field as the particle moves across the reversal layer — a clear signature of the $\mathbf{E} \times \mathbf{B}$ interaction.

Beyond the kinetic energy modulation, the radial electric field also profoundly affects the adiabaticity of alpha particle orbits. In the absence of the field, increasing the injection radius from $R_0 = 1.0$ m to $R_0 \geq 1.5$ m causes the magnetic moment μ to transition

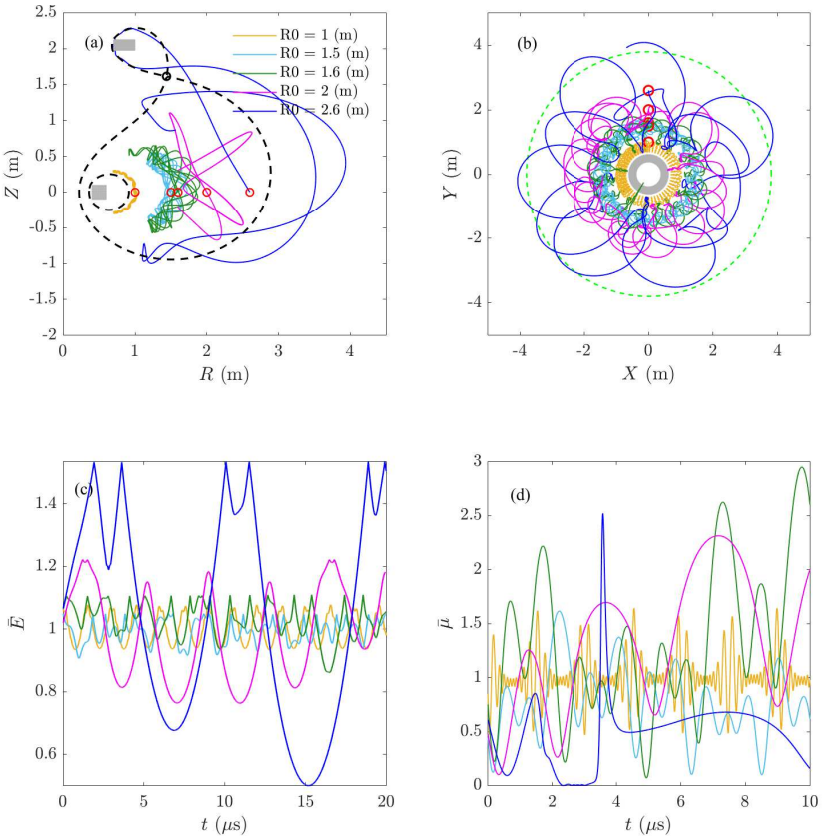


Figure 5: After increasing the radial electric field, the high-energy α particles at five different throwing points with a throwing angle of 30° are (a) in the RZ plane trajectory, (b) α particles in the Cartesian coordinate system. The orbital top view, α particles (c) kinetic energy and (d) normalized magnetic moment distribution over time. The radial electric field compresses the orbit width and introduces periodic kinetic energy modulation via $\mathbf{E} \times \mathbf{B}$ work.

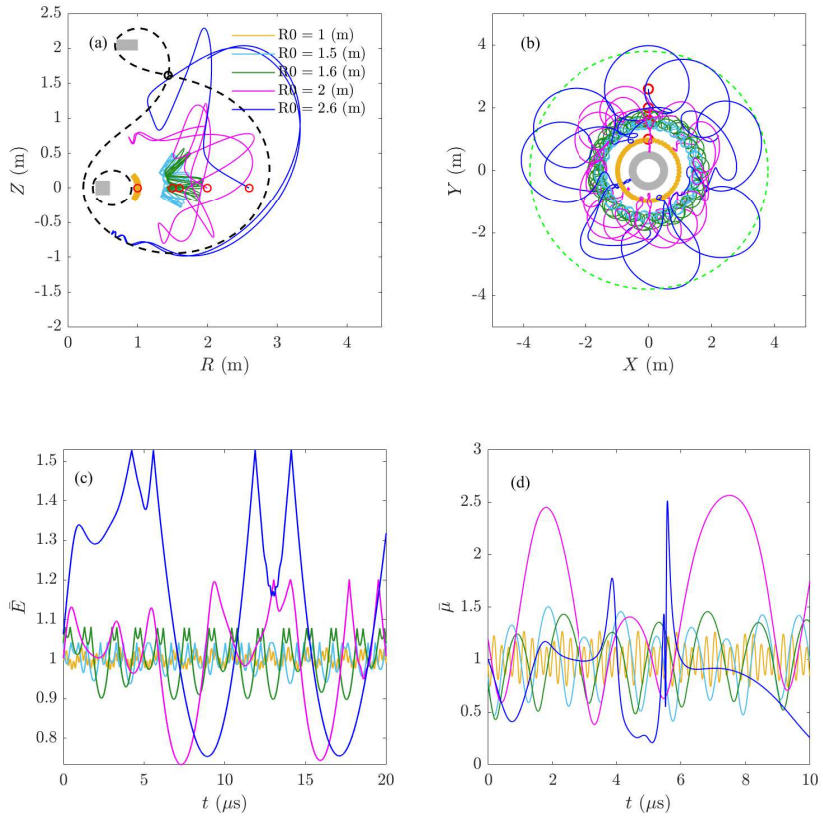


Figure 6: After increasing the radial electric field, the high-energy α particles at five different throwing points with a throwing angle of 60° are (a) in the RZ plane trajectory, (b) α particles in the Cartesian coordinate system. The orbital top view, α particles (c) kinetic energy and (d) normalized magnetic moment distribution over time.

from quasi-periodic to chaotic (Figs. 3d,4d), signaling the breakdown of adiabatic invariance. When the radial electric field is applied ($E_{\text{in}} = E_{\text{out}} = 5$ kV/m), the previously chaotic $\mu(t)$ returns to a quasi-periodic pattern (Figs. 5d,6d). The field thus acts as an "adiabaticity restorer": the $\mathbf{E} \times \mathbf{B}$ drift effectively modifies the particle's bounce-averaged radial position, restoring an approximate invariant akin to the canonical toroidal momentum. The enhanced confinement can thus be understood as a transition back toward regular, adiabatic motion.

This interpretation is quantitatively consistent with classical drift theory. For our parameters ($E_{\text{in}} = 5$ kV/m, $B \approx 0.05$ T), $v_E \approx 1 \times 10^5$ m/s, while the gradient drift $v_{\nabla B} \approx (mv_\perp^2)/(2qBR) \sim 0.5 \times 10^5$ m/s. The two drifts are comparable in magnitude, allowing $\mathbf{v}_E$ to cancel or enhance $\mathbf{v}_{\nabla B}$ and thereby compress the radial orbit width. Hence the radial electric field not only modulates kinetic energy but also restores adiabaticity, which is the physical origin of the improved confinement.

4 PARAMETER VARIATION AFFECTS CONFINEMENT

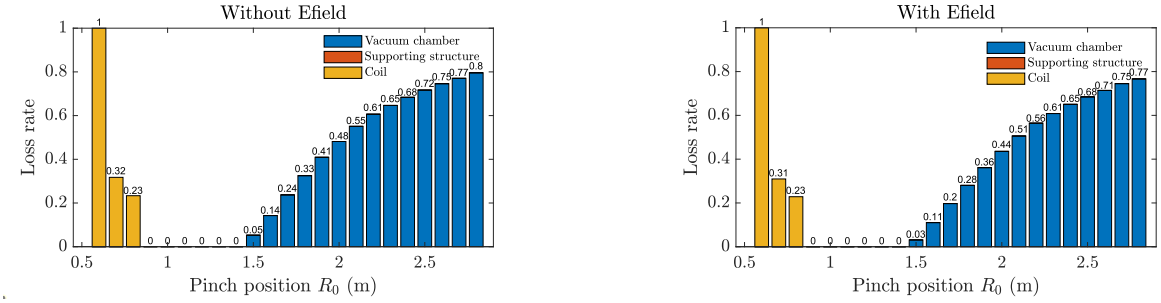
The radial electric field is characterized by three independent parameters: the inner field strength E_{in}, the outer-to-inner field ratio $\kappa = E_{\text{out}}/E_{\text{in}}$, and the reversal layer radius R_e. Each parameter influences alpha particle confinement in a distinct way: (i) E_{in} sets the overall magnitude of the $\mathbf{E} \times \mathbf{B}$ drift; (ii) κ determines the asymmetry of the "push-pull" effect across the reversal layer; and (iii) R_e controls whether the electric field acts primarily in the strong-field (small R_e) or weak-field (large R_e) region. In this section, we isolate each parameter and examine its effect on the confined fraction. The injection radius R_0 is also scanned to separate the role of the launch position from the electric field parameters.

4.1 Particle injection location

The particle loss is closely related to the injection location, therefore we have studied the confinement of alpha particles injected at different locations. We selected 23 injection locations on the mid-plane with radii ranging from 0.6 m to 2.8 m, and chose the alpha particle kinetic energy range of between 10 and 50 keV, and the injection angle range of between $-90°$ and $90°$. In total, 23,552 particles were thrown. It is assumed that particle loss channels include collisions with the vacuum chamber wall, collisions with the coil, and collisions with the support rod. The radial electric field direction conversion layer is at $R_e = 1.5$ m, with the electric field $E_{\text{in}} = E_{\text{out}} = 5$ kV/m, the time step $dt = 1 \times 10^{-10}$ s, and the particle simulation time $T = 2 \times 10^{-4}$ s. Figure 7 shows the probability of alpha particle loss as a function of radius under conditions with and without the radial electric field included.

The dipole field coil radius of the CAT-1 being 0.5 m, when alpha particles are injected at a position $R_0 = 0.6$ m on the Y-Z plane, they will collide with the coil and be lost regardless of the angle and kinetic energy of the injection. As the injection point moves away from the dipole field coil, the probability of coil collision loss decreases. When the injection point is located at R_0 ranging from 0.9 m to 1.4 m, alpha particles are confined beyond 2×10^{-4} s. When R_0 increases to 1.5 m, particles begin to be lost due to collisions with the vacuum chamber wall. In the simulation, the addition of an electric

field will not affect the collisional loss of alpha particles where particles pinch positions are near the D coil. However, in the weak magnetic field area far from the coil, the radial electric field will reduce the loss of alpha particles colliding with the vacuum chamber. The effect is significant when the injection position $R_0 = 1.5$ m, with the fraction of confined particles increasing by 40% compared to the case without the electric field. As the injection position R_0 increases, the fraction of particle confinement improved by the addition of the electric field decreases to 4%.



(a) Without radial electric field

(b) With radial electric field

Figure 7: The loss rate of particles with and without radial electric field as a function of throwing position.

4.2 Difference in electric field strength inside and outside the conversion layer

In the previous chapter, we used the same field strength inside and outside the direction conversion layer to study particle confinement. In experiments, it is not easy to achieve such a uniform field strength scenario. Therefore, this section investigates the influence of different electric field strengths inside and outside the conversion layer on the confinement of high-energy alpha particles.

Here, we keep E_{in} and scan E_{out} with the fixed ratio of internal-to-external field strength. E_{in} are selected as 0.5 kV/m, 2 kV/m, and 5 kV/m, and for each E_{in} value, the ratio of E_{out} to E_{in}, denoted as κ, is scanned from 0.5 to 2. It is assumed that the electric field direction conversion layer radius is $R_e = 2$ m. Three injection positions R_0 are selected as 1.5 m, 2 m, and 2.5 m, ensuring that there is an injection point inside, outside, and on the layer. The injection angle range is 0° to 180°, and the initial kinetic energy range is 10 keV to 50 keV. The time step is $dt = 1\times10^{-10}$ s, the simulation duration $T = 2 \times 10^{-4}$ s, and it is assumed that particles have three collision loss channels. The simulation results of the particle flight time and distance are shown in Figure 8.

Firstly, when the particle injection point is located on the conversion layer, the constrained fraction is relatively better than that of injection points located inside or outside the conversion layer. When the injection point is in the region of strong magnetic field, the collision loss of particles on the inner side of the conversion layer is essentially unaffected by the radial electric field.

Secondly, the confined time is significantly affected by the E_{in} value. Figure 8 shows the flight time and flight length of alpha particles from top to bottom for E_{in} values of 0.5 kV/m, 2 kV/m, and 5 kV/m. At the same flight time, the particle confinement fraction increases with the increase of E_{in}. In the case of $\kappa = 0.5$, when the injection point

is located in the region of weak magnetic field strength, the particle confinement fraction improves by approximately 38% at high radial electric field strengths compared to low electric field conditions. At $R_0 = 2.5$ m and $R_0 = 1.5$ m, the particle confinement fraction increases by about 33% and 12%, respectively. Under the condition of a constant internal electric field E_{in}, as κ increases, the confinement fraction of particles significantly increases at the pinch positions $R_0 = 2$ and 2.5 m. This indicates that when E_{out} is greater than E_{in}, the confinement fraction of alpha particles is enhanced. When the internal electric field $E_{\text{in}} = 5$ kV/m, the particle confinement fraction at the pinch points on the outside of the layer will be higher than that at the pinch points on the inside of the layer as the particle flight time increases. Moreover, this phenomenon becomes more pronounced with the significant increase in electric field strength. A model incorporating a radial electric field dramatically modifies the manner in which the dipole field configuration confines alpha particles. Both the intensity of the electric field and the value of κ are critical factors that determine the degree of alpha particle confinement.

The dependence on $\kappa = E_{\text{out}}/E_{\text{in}}$ can be understood through an effective potential well model. The radial electric field gives rise to an electrostatic potential $\Phi(r) = -\int E_r dr$, which has an extremum at the reversal layer R_e because E_r changes sign. When $\kappa > 1$, the potential variation outside the layer is larger than that inside, creating an asymmetric well. A particle crossing the layer experiences a net well depth $\Delta\Phi \propto (E_{\text{out}} - E_{\text{in}})\Delta r$. The confinement fraction increases with κ (Fig. 8), and raising κ from 1 to 2 yields an additional $\sim 12\%$ improvement (Fig. 10). This gain is attributed to deeper trapping that further suppresses radial drift. Thus κ is the control parameter that determines the net "push-pull" effect, suggesting that deliberately creating $\kappa > 1$ profiles (e.g., by coil biasing or ECRH modulation) could enhance alpha confinement in experiments.

4.3 Radial electric field conversion layer radius

In actual experiments, the position of the electric field direction conversion layer may change due to the presence of various frequencies of electron cyclotron heating (ECRH) beams in the device. Therefore, the influence of the radial electric field conversion layer radius on the alpha particle orbit is studied. Here, we set the injection position R_0 as a scanning parameter with a range between 0.7 m and 2.7 m, thereby excluding interference from the relationship between the injection position and the conversion layer on the confinement fraction. Here, we assume the conversion layer radius R_e to be 0 m, 1 m, and 2 m, respectively. For each R_e parameter, we select injection angles of 0° and 180°, and the particles have an initial kinetic energy of 25 keV. In this section, we choose κ to be 0.5, 1, and 2 with fixed E_{in} to investigate characteristics of the particle confinement. We assume a time step $dt = 1 \times 10^{-10}$ s and a total duration $T = 2 \times 10^{-4}$ s, with particles having three collision loss channels.

The first to third rows of Figure 9 show the trends of particle fraction variation with flight time (first column) and flight distance (second column) under the conditions where the inner layer electric field E_{in} is 0.5, 2, and 5 kV/m, respectively. When the intensity of the inner electric field E_{in} is 0.5 kV/m, the particle confinement fraction basically does not change with variations in R_e and κ. However, as E_{in} increases, different values of R_e and κ will have a certain distinguishing effect on the particle confinement fraction curves.

Figure 10 provides a detailed view of the particle confinement fraction as it changes with flight time at a constant E_{in} of 5 kV/m. It is observed that when $E_{\text{in}} = E_{\text{out}}$, the particle confinement fraction is sensitive to variations in the value of R_e. As R_e

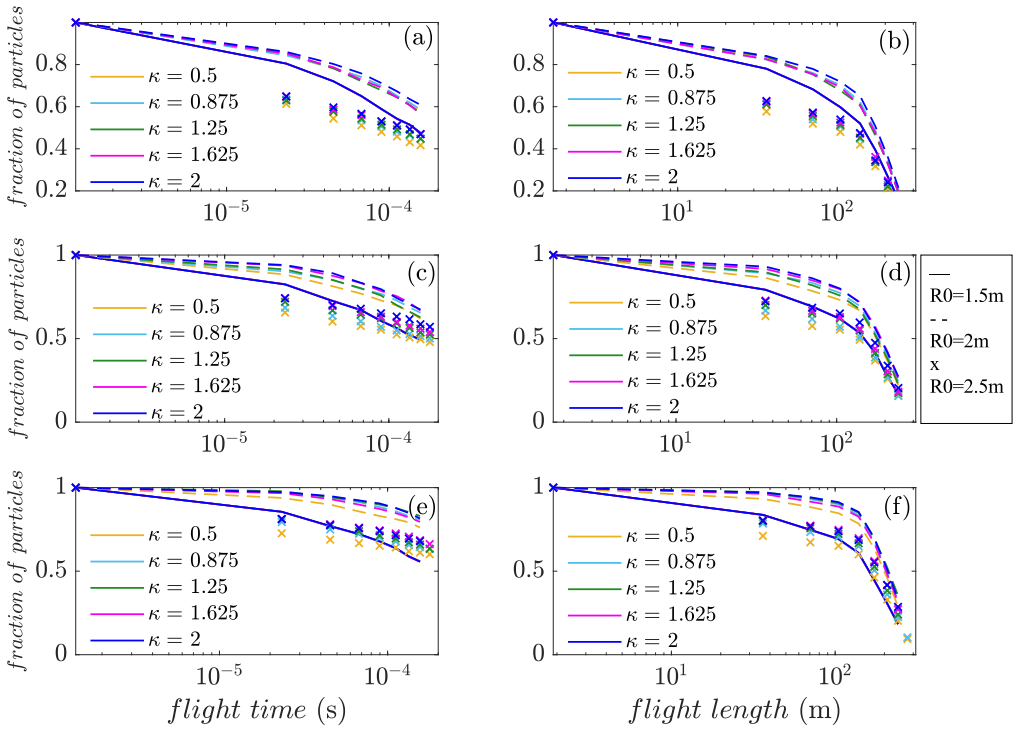


Figure 8: The variation in the flight time of α particles (a) and the proportion of particle flight length (b) when the throwing position R_0 is 1.5 m, 2 m, and 2.5 m in the radial electric field transition layer ($R_e = 2$ m) with an internal field strength of 500 V/m. (c,d) Internal field strength of 2 kV/m. (e,f) Internal field strength of 5 kV/m.

increases, there is a noticeable enhancement in the particle confinement fraction. At a value of $\kappa = 0.5$, the particle confinement fractions for $R_e = 1$ and $R_e = 2$ converge at 0.2 ms, suggesting a trend towards saturation in the enhancement of particle confinement as the transition layer radius grows. With $R_e = 2$ m, the particle confinement fraction is approximately 6% greater than at $R_e = 0$, and as κ increases, the maximum particle confinement fraction could potentially be enhanced by up to 12%.

In order to investigate the background plasma being heated by the collision of alpha particles, we compare the slowing down time and confinement time of alpha particles in CAT-1. The slowing-down time [10, 16] $\tau_{\alpha i}$ for alpha particles colliding with background plasma ions is

$$\tau_{\alpha i} = \frac{4\pi\epsilon_0^2 M M_b V^3}{n_i Z^2 Z_b^2 e^4 \ln\Lambda} \approx 1.4 \times 10^{-8} \text{ s}. \tag{11}$$

This result indicates that the slowing-down time is much shorter than the confinement time of alpha particles. This implies that even alpha particles with very high kinetic energy can lose energy quickly through collisions with ions in the background plasma and be captured by the magnetic dipole field.

Nevertheless, the 40% improvement in the confined fraction due to the radial electric field remains significant for plasma heating. The reason lies in the high-energy tail of the alpha particle distribution. Slowing-down is not mono-energetic; alphas with initial energies of 10–50 keV that have undergone fewer collisions retain higher energies for a longer time. Such high-energy particles have larger Larmor radii and stronger drifts, making them the most prone to loss. The radial electric field compresses their orbits, preferentially retaining this tail. Consequently, the enhanced confinement fraction directly prolongs the energy deposition time of the most energetic alphas, contributing to more efficient background plasma heating even when the average slowing-down time is short. This clarifies why electric field tuning can significantly improve overall heating efficiency.

5 CONCLUSIONS

We have systematically investigated the effect of a radial electric field — motivated by observations in LDX and other dipole devices — on the confinement of high-energy alpha particles in the CAT-1 levitated dipole experiment. Using test-particle simulations that include realistic loss channels (vacuum chamber, support rods, and the floating coil), we arrive at three main conclusions.

First, the presence of a moderate radial electric field ($E_{\text{in}} \approx 5$ kV/m, $\kappa = 1$) significantly improves alpha particle confinement. Compared to the field-free case, the confined fraction increases by up to 40% for particles injected near the reversal layer ($R_0 \approx 1.5$ m), and by 4–12% for other injection radii. The improvement is most pronounced in the weak-field region outside the coil, where the magnetic field alone is insufficient to confine alphas.

Second, the confinement fraction depends sensitively on both the magnitude of the inner field E_{in} and the ratio $\kappa = E_{\text{out}}/E_{\text{in}}$. At $\kappa = 0.5$, increasing E_{in} from 0.5 to 5 kV/m raises the confined fraction by approximately 38% (for $R_0 = 2.5$ m). For a fixed E_{in}, increasing κ from 0.5 to 2 yields an additional enhancement of up to 12%, especially when the reversal layer is located at $R_e = 2$ m. These scalings suggest that an asymmetric "push-pull" electric field ($|E_{\text{out}}| > |E_{\text{in}}|$) is more effective at compressing alpha particle

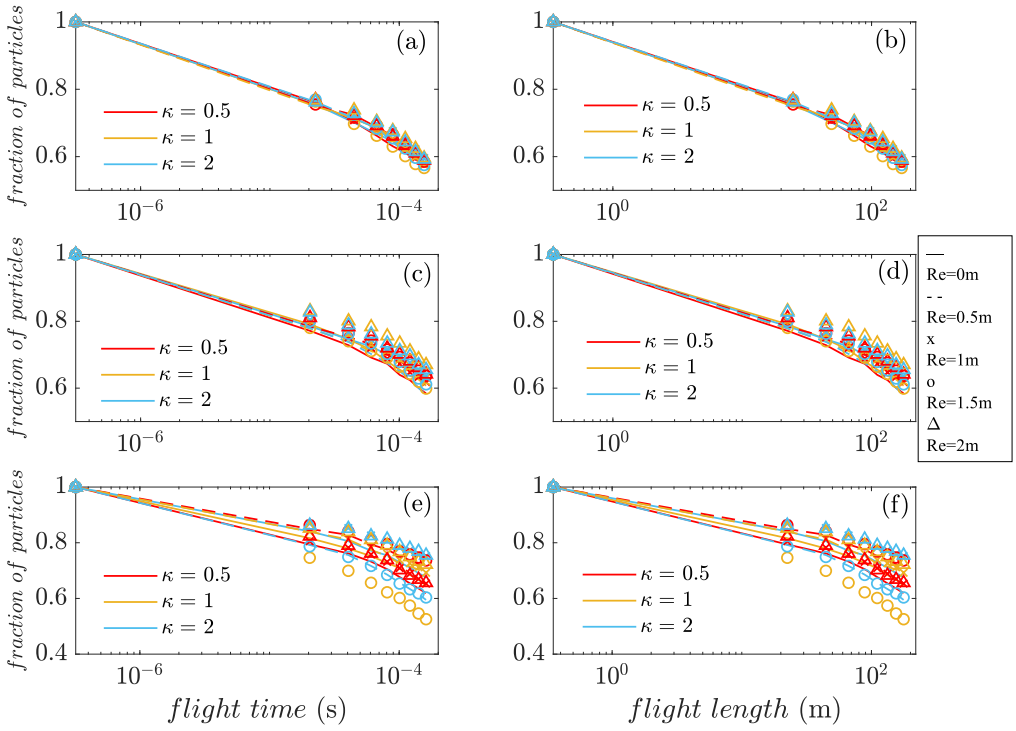


Figure 9: When the α particle changes in the radial electric field conversion layer, (a) the internal field strength is 500 V/m: particle flight time, (b) proportion of particle flight length; (c,d) internal field strength 2 kV/m; (e,f) internal field strength 5 kV/m.

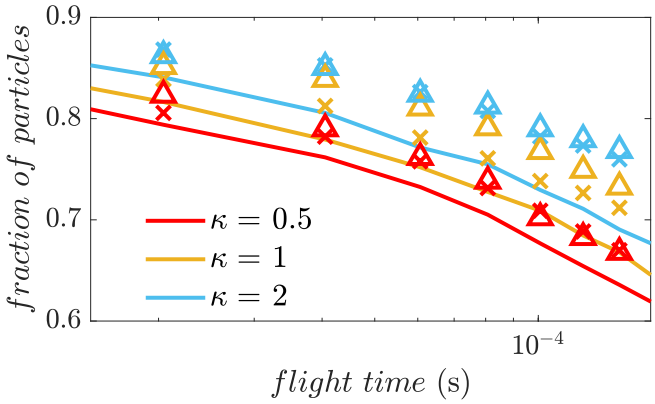


Figure 10: When the internal field strength is 5 kV/m, the proportion of particles changes with the flight time of particles.

orbits.

Third, the role of the reversal layer radius R_e is secondary to $E_{\rm in}$ and κ, but still non-negligible. At high $E_{\rm in}$ (5 kV/m), increasing R_e from 0 to 2 m improves the confined fraction by 6–12%, with the effect saturating beyond $R_e \approx 2$ m. This saturation indicates that once the reversal layer is placed sufficiently far out in the weak-field region, further outward movement does not provide additional benefit.

In summary, the radial electric field improves alpha particle confinement by (i) restoring adiabatic invariance in the weak-field region, (ii) creating an asymmetric potential well (with $\kappa > 1$) that compresses orbits, and (iii) preferentially retaining the high-energy tail of the distribution. These three physical mechanisms, all supported by the simulation data, demonstrate that the radial electric field is not merely a parasitic effect but a versatile tool for controlling alpha heating in dipole devices.

Limitations and outlook

The present test-particle model neglects collective plasma effects (e.g., self-consistent electric field evolution, wave-particle interactions) and Coulomb collisions with background ions. Although we estimated the alpha-ion slowing-down time to be much shorter than the confinement time ($\tau_{\alpha i} \approx 1.4 \times 10^{-8}$ s vs. simulation time 2×10^{-4} s), a fully self-consistent kinetic description would be needed to capture the feedback between alpha particles and the background plasma. Future work will extend the present analysis to include gyrokinetic or particle-in-cell simulations, and will explore whether tailored radial electric field profiles can be actively generated (e.g., by biased electrodes or electron cyclotron current drive) to optimize alpha particle heating in next-step dipole devices such as CAT-1.

Implications for dipole fusion

The results demonstrate that the radial electric field is not merely a parasitic effect but a potentially tunable parameter for controlling alpha particle orbits. By adjusting the strength and asymmetry of the radial electric field — possibly through biasing of the floating coil or by modulating ECRH power — one could enhance alpha heating efficiency and reduce losses to the chamber wall. This provides a novel, knob-like control mechanism that could be exploited in future dipole-based fusion reactors.

Acknowledgments

Supported by Engineering Research Center of Nuclear Technology Application (East China Institute of Technology), Ministry of Education (No. HJSJYB2022-1); National Natural Science Foundation of China (Grant No. 52261042); National Natural Science Foundation of China (Grant No. 12105042); Double Thousand Plan of Jiangxi Province (Jiangxi Double Thousand Plan) (DHSOT22021001).

References

[1] A. Hasegawa, "A dipole field fusion reactor," Comments on Plasma Physics and Controlled Fusion **11**, 147–151 (1987).

[2] A. Hasegawa, L. Chen, and M. E. Mauro, "A D-3He fusion reactor based on a dipole magnetic field," Nuclear Fusion **30**(11), 2405 (1990); https://doi.org/10.1088/0029-5515/30/11/018.

[3] A. Boxer, R. Bergmann, J. L. Ellsworth, D. T. Garnier, J. Kesner, M. E. Mauro, and P. Woskov, "Turbulent inward pinch of plasma confined by a levitated dipole magnet," Nature Physics **6**, 207–212 (2010); https://doi.org/10.1038/nphys1510.

[4] Z. Yoshida, Y. Ogawa, J. Moriyama, S. Watanabe, Y. Yano, S. Mizumaki, T. Sugawara, and K. Ito, "First plasma in the RT-1 device," Plasma and Fusion Research **1**, 008–008 (2006); https://doi.org/10.1585/pfr.1.008.

[5] A. Kouznetsov, J. Kesner, and D. Garnier, "Theoretical prediction of τ_E and β in a large aspect ratio LDX," Massachusetts Institute of Technology (2007).

[6] T. M. Roberts, "Local regulation of interchange turbulence in a dipole-confined plasma torus using current injection feedback," Columbia University (2015).

[7] C. G. Fälthammar, "Effects of time-dependent electric fields on geomagnetically trapped radiation," Journal of Geophysical Research **70**(11), 2503–2516 (1965); https://doi.org/10.1029/JZ070i011p02503.

[8] L. Guazzotto, R. Betti, J. Kesner, and J. J. Ramos, "Equilibrium beta limits in a dipole configuration," Physics of Plasmas **14**(6) (2007); https://doi.org/10.1063/1.2736676.

[9] Z. Wang, Y. Liu, and G. Zhang, "Magnetic field configuration of attitude control coil based on line segment approximation method," Nuclear Techniques **47**(04), 040504 (2024) (in Chinese); https://dx.doi.org/10.11889/j.0253-3219.2024.hjs.47.040504.

[10] A. S. Richardson, "2019 NRL plasma formulary," Naval Research Laboratory, Washington, DC (2019).

[11] J. Kesner, D. Garnier, A. Hansen, M. Mauro, and A. Simakov, "Helium catalysed D–D fusion in a levitated dipole," Nuclear Fusion **44**(1), 193 (2003); https://doi.org/10.1088/0029-5515/44/1/021.

[12] M. Abler, "Characterizing Intermittent Turbulent Wave Kinetics and Energy Transfer via Three-Wave Coupling in Dipole-Confined Plasma," Columbia University (2021).

[13] Q. Hong, Y. Wang, and Y. Xiao, "Why is Boris algorithm so good?" Physics of Plasmas **20**, 084503 (2013); https://doi.org/10.1063/1.4818428.

[14] J. P. Boris, "Proceedings, Fourth Conference on the Numerical Simulation of Plasmas," Naval Research Laboratory, Washington, D.C. (1971).

[15] Y. Omura, "One-dimensional electromagnetic particle code," in *Proceedings of ISSS*, Vol. 7, pp. 26–31 (2005).

[16] R. J. Goldston and P. H. Rutherford, *Introduction to Plasma Physics* (1995).